

Analysis and Design of Hybrid and Graphene-Based Plasmonic Waveguide Components

D. A. Ketzaki, V. Salonikios, I. Demirtzioglou and T. V. Yioultsis

*Dept. of Electrical and Computer Engineering, Aristotle University of Thessaloniki, Thessaloniki, Greece
traianos@auth.gr*

Keywords: Graphene, plasmonics, plasmonic waveguides, hybrid waveguides.

Abstract: We present an efficient finite element formulation for the eigenmode analysis of graphene-based plasmonic waveguides with switching functionalities. The formulation is full-vectorial and addresses graphene as a surface conductivity, as opposed to bulky material considerations, thus eliminating the need for fine discretizations inside thin graphene models. Based on this technique, several graphene-enhanced plasmonic waveguides and components with promising characteristics are proposed.

1 INTRODUCTION

Graphene is a relatively new innovative material, with interesting new physics and several significant properties and effects, including the ability to support surface plasmon propagating modes and switching functionalities (Bludov et al., 2013). Optical conductivity of graphene has been shown to consist of a Drude intraband term and an interband contribution. These properties may result in either plasmonic modes in THz (Nikitin et al., 2011) or enhanced switching in photonic waveguides for the optical communications regime (Sun et al., 2014). In particular, for the case of the THz regime, where the Drude term is dominant, graphene surface plasmons offer the possibility of waveguiding with strong confinement, while in the optical communications spectrum where the interband contribution is substantial, the tunability of graphene's conductivity through electrostatic gating shows great potential for the design of switching components.

As for the analysis and design of graphene-based and enhanced waveguides and components, the finite element method (FEM) is a perfect candidate, due to its ability to deal with problems of considerable geometric complexity. However, the general trend is often to approach graphene as a bulky material, thus requiring very fine discretizations inside thin sheets and the surrounding space as well. We present here an efficient formulation for both the eigenmode and the 3D analysis of graphene-based plasmonic waveguides and components with switching functionalities

which is full-vectorial and addresses graphene as a thin sheet with a surface conductivity. Based on this analysis, we propose a graphene-enhanced plasmonic CGS waveguide with an extinction ratio of 8.6 dB and a 2.15 dB insertion loss for a 10 μm length, which can be considered highly satisfactory. A particular investigation of a three-dimensional microring /microdisk filter reveals the possibility of actual designs with extinction ratios exceeding 10 dB, which is also a firm basis for further study towards the development of switched plasmonic components in the photonics regime.

2 FINITE ELEMENT FORMULATION

The proposed finite element eigenmode formulation follows the general framework that has been proposed in (Selleri et al., 2001), where the electric field is used as a working variable. The formulation uses mixed finite elements for the discretization of the waveguide cross section, with tangentially continuous (H-curl) vector finite elements in the transverse plane and scalar (nodal) finite elements for the axial component. Using the Galerkin formulation for the Helmholtz equation, the form

$$\iint_S \mathbf{E}' \cdot \left(\nabla \times \overline{\mu}_r^{-1} \nabla \times \mathbf{E} - k_0^2 \overline{\varepsilon}_r \mathbf{E} \right) ds = 0 \quad (1)$$

expresses the projected problem, reducing its solution to a finite-dimensional vector subspace. The

electric field can be written in the form $\mathbf{E} = (\mathbf{E}_t + \hat{\mathbf{z}}E_z)e^{-\gamma z}$, where $\mathbf{E}_t = \mathbf{E}_t(x, y)$ represents the transverse component and $E_z = E_z(x, y)$ represents the axial component. The adjoint field $\mathbf{E}' = (\mathbf{E}'_t - \hat{\mathbf{z}}E'_z)e^{\gamma z}$ is selected as the test function in the Galerkin equation and the final eigenmode formulation expressed as a function of the effective refractive index $n_{eff} = -j\gamma / k_0$ is as follows:

$$\begin{aligned} & \iint_S \nabla \times \mathbf{E}'_t \cdot \mu_{r,zz}^{-1} \nabla \times \mathbf{E}_t ds \\ & - \iint_S (\nabla E'_z \times \hat{\mathbf{z}}) \cdot \overline{\mu_{r,tt}^{-1}} (\nabla E_z \times \hat{\mathbf{z}}) ds \\ & - k_0^2 \iint_S \mathbf{E}'_t \cdot \overline{\epsilon_{r,tt}} \mathbf{E}_t ds + k_0^2 \iint_S E'_z \cdot \epsilon_{r,zz} E_z ds \\ & + n_{eff} \begin{bmatrix} -jk_0 \iint_S (\mathbf{E}'_t \times \hat{\mathbf{z}}) \cdot \overline{\mu_{r,tt}^{-1}} (\nabla E_z \times \hat{\mathbf{z}}) ds \\ -jk_0 \iint_S (\nabla E'_z \times \hat{\mathbf{z}}) \cdot \overline{\mu_{r,tt}^{-1}} (\mathbf{E}_t \times \hat{\mathbf{z}}) ds \end{bmatrix} \\ & + n_{eff}^2 \begin{bmatrix} k_0^2 \iint_S (\mathbf{E}'_t \times \hat{\mathbf{z}}) \cdot \overline{\mu_{r,tt}^{-1}} (\mathbf{E}_t \times \hat{\mathbf{z}}) ds \\ - \iint_{\partial S} \mathbf{E}' \cdot \hat{\mathbf{n}} \times \nabla \times \mathbf{E} ds = 0 \end{bmatrix} \end{aligned} \quad (2)$$

The domain is terminated by perfectly matched layers. Following the discretization of the 2D-space, using basis functions and the degrees of freedom (nodal or edge-based, according to the field component) for the electric field quantities and assuming for the moment that the line integral vanishes, (2) leads to the quadratic eigenvalue problem expanded form of Galerkin formulation,

$$\begin{bmatrix} \mathbf{S}' - k_0^2 \mathbf{T}' & 0 \\ 0 & -\mathbf{S}^{z,m} + k_0^2 \mathbf{T}^z \end{bmatrix} \begin{bmatrix} \mathbf{E}_t \\ \mathbf{E}_z \end{bmatrix} + n_{eff} \begin{bmatrix} 0 & -jk_0 \mathbf{P} \\ -jk_0 \mathbf{Q} & 0 \end{bmatrix} \begin{bmatrix} \mathbf{E}_t \\ \mathbf{E}_z \end{bmatrix} + n_{eff}^2 \begin{bmatrix} k_0^2 \mathbf{T}^{t,m} & 0 \\ 0 & 0 \end{bmatrix} \begin{bmatrix} \mathbf{E}_t \\ \mathbf{E}_z \end{bmatrix} = 0 \quad (3)$$

Where

$$\begin{aligned} S'_{ij} &= \iint_{S_n} \nabla \times \mathbf{w}_i \cdot \mu_{r,zz}^{-1} \nabla \times \mathbf{w}_j ds, \\ S^{z,m}_{ij} &= \iint_{S_n} (\nabla N_i \times \hat{\mathbf{z}}) \cdot \overline{\mu_{r,tt}^{-1}} (\nabla N_j \times \hat{\mathbf{z}}) ds, \\ T'_{ij} &= \iint_{S_n} \mathbf{w}_i \cdot \overline{\epsilon_{r,tt}} \mathbf{w}_j ds, T^{z,z}_{ij} = \iint_{S_n} N_i \cdot \epsilon_{r,zz} N_j ds, \\ T^{z,m}_{ij} &= \iint_{S_n} (\mathbf{w}_i \times \hat{\mathbf{z}}) \cdot \overline{\mu_{r,tt}^{-1}} (\mathbf{w}_j \times \hat{\mathbf{z}}) ds, \\ P_{ij} &= \iint_{S_n} (\mathbf{w}_i \times \hat{\mathbf{z}}) \cdot \overline{\mu_{r,tt}^{-1}} (\nabla N_j \times \hat{\mathbf{z}}) ds, \\ Q_{ij} &= \iint_{S_n} (\nabla N_i \times \hat{\mathbf{z}}) \cdot \overline{\mu_{r,tt}^{-1}} (\mathbf{w}_j \times \hat{\mathbf{z}}) ds \end{aligned} \quad (4)$$

To solve the quadratic eigenvalue problem we use first companion linearization to reduce it to

$$\begin{bmatrix} 0 & 0 & \mathbf{I} & 0 \\ 0 & 0 & 0 & \mathbf{I} \\ -\mathbf{S}' + k_0^2 \mathbf{T}' & 0 & 0 & jk_0 \mathbf{P} \\ 0 & \mathbf{S}^{z,m} - k_0^2 \mathbf{T}^z & jk_0 \mathbf{Q} & 0 \end{bmatrix} \begin{bmatrix} \mathbf{E}_t \\ \mathbf{E}_z \\ n_{eff} \mathbf{E}_t \\ n_{eff} \mathbf{E}_z \end{bmatrix} = n_{eff} \begin{bmatrix} \mathbf{I} & 0 & 0 & 0 \\ 0 & \mathbf{I} & 0 & 0 \\ 0 & 0 & k_0^2 \mathbf{T}^{t,m} & 0 \\ 0 & 0 & 0 & 0 \end{bmatrix} \begin{bmatrix} \mathbf{E}_t \\ \mathbf{E}_z \\ n_{eff} \mathbf{E}_t \\ n_{eff} \mathbf{E}_z \end{bmatrix} \quad (5)$$

which is a sparse form with a positive semidefinite matrix at the right hand side, suitable for sparse eigensolvers.

As far as the graphene implementation is concerned, its extremely small thickness (one-atom thick) dictates its consideration as an ideal two-dimensional surface with a corresponding surface conductivity σ_g (measured in S). Therefore, any graphene surfaces in the waveguide eigenmode analysis are basically represented by one-dimensional lines in the 2D cross-section of the structures (Figure 1).

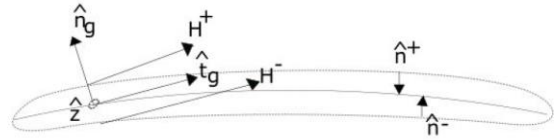


Figure 1: Representation of graphene as an infinitely thin sheet (2D cross section) and its surrounding surface.

A first route to incorporate graphene sheets in FEM simulations is to start from a bulky material approach and consider the limit of its thickness to zero. In this case, graphene's contribution would be apparent through its conductivity, thus affecting the 3rd and 4th term of (2) which include permittivity quantities. In these integrals, separating a finite surface of thickness δ corresponding to the bulky graphene area, we derive the additional terms

$$I_g = -k_0^2 \iint_{S_1} \mathbf{E}'_t \cdot \overline{\overline{\boldsymbol{\varepsilon}_{r,tt}}} \mathbf{E}_t ds + k_0^2 \iint_{S_1} E'_z \cdot \boldsymbol{\varepsilon}_{r,zz} E_z ds \quad (6)$$

where we replace the permittivity with the complex permittivity of graphene $\boldsymbol{\varepsilon}_r^* = \boldsymbol{\varepsilon}_r - j\boldsymbol{\sigma}_b / \omega\boldsymbol{\varepsilon}_0$, and $\boldsymbol{\sigma}_b$ describes an equivalent conductivity of bulk graphene (in S/m). Assuming that $\boldsymbol{\sigma}_b$ consists of non-zero real and imaginary parts, we can omit $\boldsymbol{\varepsilon}_r$ as being included in $\boldsymbol{\sigma}_b$ and have $\boldsymbol{\varepsilon}_r^* = -j\boldsymbol{\sigma}_b / \omega\boldsymbol{\varepsilon}_0$. Therefore (6) becomes

$$I_g = jk_0\eta_0 \iint_{S_1} \mathbf{E}'_t \cdot \boldsymbol{\sigma}_b \mathbf{E}_t ds - jk_0\eta_0 \iint_{S_1} E'_z \cdot \boldsymbol{\sigma}_b E_z ds \quad (7)$$

Assuming an infinitesimal graphene thickness, variations are negligible in this dimension, giving

$$I_g = jk_0\eta_0 \int_{\partial S} \mathbf{E}'_{t,p} \cdot \boldsymbol{\sigma}_g \mathbf{E}_{t,p} dl - jk_0\eta_0 \int_{\partial S} E'_z \cdot \boldsymbol{\sigma}_g E_z dl \quad (8)$$

where $\delta\boldsymbol{\sigma}_b$ equals the surface conductivity $\boldsymbol{\sigma}_g$ (in S). It has to be particularly noted that the electric field component $\mathbf{E}_{t,p}$ involved in the first integral is not the full transverse component but only its tangential projection on the one-dimensional graphene line.

An equivalent and more elegant way to arrive at the same expression is to consider graphene as a zero thickness sheet in the first place. In this case, the line integral term in (2) cannot be ignored, as the graphene current sheet introduces a discontinuity in the magnetic field, thus affecting the line integral term. In particular, the interface condition on the graphene sheet is written in the form

$$\begin{aligned} & -\frac{j}{k_0\eta_0} (\hat{\mathbf{n}}_g \times \nabla \times \mathbf{E}^+ - \hat{\mathbf{n}}_g \times \nabla \times \mathbf{E}^-) \\ & = \mathbf{J}_s = \boldsymbol{\sigma}_g (\mathbf{E}_{t,p} + \hat{\mathbf{z}} E_z) \end{aligned} \quad (9)$$

where $\hat{\mathbf{n}}_g$ is the unit vector normal to the graphene sheet. However, to substitute (9) in the line integral term of (2) we need to consider a fictitious surface that surrounds the graphene sheet from both sides and being infinitely close to it. Therefore, the line integral is split into two parts, one for the upper surface, where the outward-pointing unit normal vector is $\hat{\mathbf{n}}^+ = \hat{\mathbf{n}}_g$ and one for the lower one, where $\hat{\mathbf{n}}^- = -\hat{\mathbf{n}}_g$ and the line integral takes the form

$$\begin{aligned} I_g &= \int_{\partial S^+} \mathbf{E}' \cdot \hat{\mathbf{n}}^+ \times \nabla \times \mathbf{E}^+ ds + \int_{\partial S^-} \mathbf{E}' \cdot \hat{\mathbf{n}}^- \times \nabla \times \mathbf{E}^- ds \\ &= \int_{\partial S^-} \mathbf{E}' \cdot \hat{\mathbf{n}}_g \times (\nabla \times \mathbf{E}^+ - \nabla \times \mathbf{E}^-) ds \\ &= jk_0\eta_0 \int_{\partial S^-} \mathbf{E}' \cdot \boldsymbol{\sigma}_g \mathbf{E}_p ds \end{aligned} \quad (10)$$

which easily results in (9) as well.

Therefore, graphene's contribution can be implemented by adding two line integral terms in the initial formulation, expressed as

$$T_e^{t,g} = \int_C \mathbf{E}'_{t,p} \cdot \boldsymbol{\sigma}_g \mathbf{E}_{t,p} dl, T_e^{z,g} = \int_C E'_z \cdot \boldsymbol{\sigma}_g E_z dl \quad (11)$$

and by considering the corresponding matrices, it results in the linear eigenvalue problem similar to (5), where the term $-jk_0\eta_0 \mathbf{T}^{t,g}$ is added to $-\mathbf{S}^t + k_0^2 \mathbf{T}^t$ and $jk_0\eta_0 \mathbf{T}^{z,g}$ is added to $\mathbf{S}^{z,m} - k_0^2 \mathbf{T}^z$.

The three-dimensional FEM formulation is similarly based on a standard Galerkin formulation with vector finite elements in three dimensions, starting from the 3D version of (2). Since there is no split in transverse and axial components, the Galerkin formulation will include only 3D forms of the first, third and last terms in (2). Following similar principles, a graphene-related term of the form $jk_0\eta_0 \mathbf{T}^g$ will be added to the standard FEM stiffness-mass matrix $\mathbf{S} - k_0^2 \mathbf{T}$.

3 PLASMONIC AND SWITCHING COMPONENTS

The proposed formulations are able to analyze both plasmon graphene ribbon waveguides in the THz regime and a switching-capable waveguide structure for telecom applications, based on the CGS waveguide (Dai and He, 2009), which is properly enhanced by graphene.

3.1 Graphene waveguide with high-index dielectric ridge

The first structure simulated was the graphene waveguide proposed in (Sun et al., 2014). Its concept takes advantage of a high-index dielectric ridge to achieve strong field confinement without using a finite width graphene ribbon which is harder to fabricate. Placing a wide graphene sheet over a dielectric ridge of appropriate size, the geometry of the structure facilitates waveguiding. The relation of the complex effective refractive index to the thickness of gap the graphene sheet and the dielectric ridge, as well as to the chemical potential are shown in Fig. 3, being in very good agreement with (Sun et al., 2014).

3.2 Graphene microribbon waveguide

To fully test the functionality of our formulation, we analyzed a plasmon graphene microribbon waveguide in the THz regime (Nikitin et al., 2011). This is a waveguiding structure for frequencies between 1 and 12 THz (as opposed to the telecommunications wavelength regime) taking advantage of the surface conductivity of a graphene microribbon. The analysis was conducted for a ribbon width of 5 μm and the electric field intensity plots for the two transverse components are shown in Figure 2.

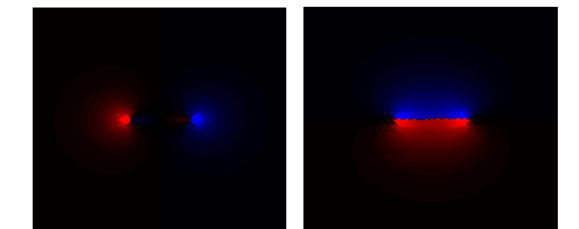
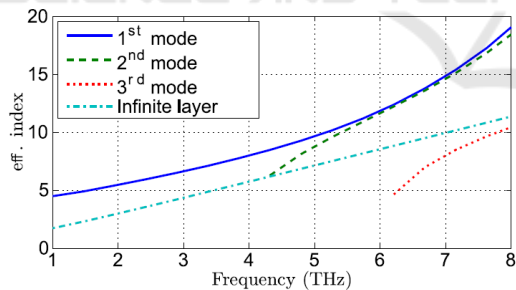


Figure 2: Effective refractive index (real part) and mode profiles for the first mode of a 5 μm graphene ribbon waveguide (vertical and horizontal E-field component, respectively).

3.3 Graphene waveguide with high-index dielectric ridge

The next structure simulated was the graphene waveguide proposed in (Sun et al., 2014). Its concept takes advantage of a high-index dielectric ridge to achieve strong field confinement without using a finite width graphene ribbon which is harder to fabricate. Placing a wide graphene sheet over a dielectric ridge of appropriate size, the geometry of the structure facilitates waveguiding. The relation of the complex effective refractive index to the thickness of gap of the graphene sheet and the dielectric ridge, as well as to the chemical potential are shown in Figure 3, being in very good agreement with (Sun et al., 2014).

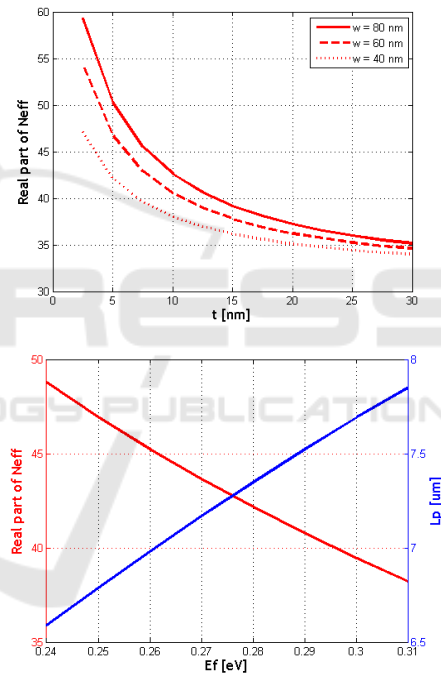


Figure 3: Real part of the effective refractive index with respect to gap thickness and chemical potential

3.4 Graphene switching component

Based on the analysis, we propose a switching capability for the classic plasmonic CGS waveguide (Dai and He, 2009), (Wu et al., 2010) by adding graphene layers on all interfaces between waveguide materials, including both sides of the oxide layer, and also the two vertical ridges of the waveguide. The ON and OFF states of the waveguide correspond to chemical potential values 1 eV and 0.1 eV. Selecting a structure length of 10 μm , the insertion loss can be as low as 2.15 dB, almost

entirely due to metal (not graphene) losses and the achieved extinction ratio is 8.6 dB, which is highly promising for further study.

3.5 Switched plasmonic components with frequency selective functionalities

Following the proposed waveguide components we further proceed to the design of three dimensional components with frequency tuning functionalities, like the waveguide-coupled microring structure of Figure 4. For more enhanced performance, the microring concept is extended to cover the cases of a microdisk or a donut-shaped ring. The component's performance, in terms of the power transmission coefficient is shown in Figure 5, for both the microdisk and donut shapes, for the ON state, while the achieved extinction ratio between ON and OFF states for the graphene enhanced component exceeds 11.5 dB, which is a figure suitable for practical considerations.

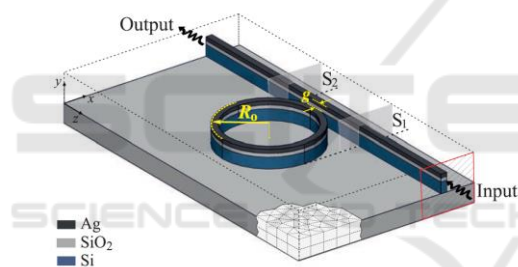


Figure 4: Microring resonator filter based on the CGS waveguide

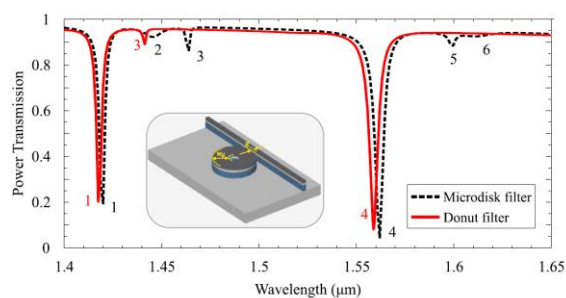


Figure 5: Frequency response of the microdisk and donut structures, in terms of the power transmission coefficient. Outer ring radius is 0.85 μm , inner ring radius for the donut structure is 0.45 μm and the gap is set to 150 nm.

4 CONCLUSIONS

We have presented a full-vectorial finite element formulation for the eigenmode analysis of graphene-based plasmonic waveguides and components with switching functionalities. The formulation addresses graphene as a surface conductivity thus eliminating the need for fine discretizations inside thin graphene sheets. Finally, several plasmonic or switched components with promising characteristics have been proposed.

REFERENCES

- Bludov, Y.V., Ferreira, A., Peres N. M. R. and Vasilevskiy M. I., "A Primer on Surface Plasmon-Polaritons in Graphene," *Int. J. Mod. Phys. B*, 27, 1341001, 2013.
- Nikitin, A. Y., Guinea, F. and Garcia-Vidal, F. J., "Edge and waveguide terahertz surface plasmon modes in graphene microribbon," *Phys. Rev. B*, 84, 161407(R), 2011.
- Sun, Y., Zheng, Z., Cheng, J. and Liu J., "Graphene surface plasmon waveguides incorporating high-index dielectric ridges for single mode transmission," *Optics Communications*, 328, pp. 124–128, 2014.
- Selleri, S., Vincetti, L., Cucinotta, A. and Zoboli, M. "Complex FEM modal solver of optical waveguides with PML boundary conditions," *Optical and Quantum Electronics*, vol. 33, no. 4-5, pp. 359-371, 2001.
- Dai, D. and He, S., "A silicon-based hybrid plasmonic waveguide with a metal cap for a nano-scale light confinement", *Optics Express*, vol. 17, no. 19, 2009.
- Wu, M., Han, Z. and Van, V., "Conductor-gap-silicon plasmonic waveguides and passive components at subwavelength scale," *Optics Express*, vol. 18, no. 11, pp. 11728-11736, 2010.